

Current effects on global motions of a floating platform in waves

Meng Shen^a and Yuming Liu*

Department of Mechanical Engineering, Massachusetts Institute of Technology, Cambridge, MA 02139, USA

(Received March 11, 2017, Revised May 28, 2017, Accepted May 30, 2017)

Abstract. The purpose of this paper is to understand and model the slow current (~ 2 m/s) effects on the global response of a floating offshore platform in waves. A time-domain numerical simulation of full wave-current-body interaction by a quadratic boundary element method (QBEM) is applied to compute the hydrodynamic loads and motions of a floating body under the combined influence of waves and current. The study is performed in the context of linearized potential flow theory that is sufficient in understanding the leading-order current effect on the body motion. The numerical simulations are validated by quantitative comparisons of the hydrodynamic coefficients with the WAMIT prediction for a truncated vertical circular cylinder in the absence of current. It is found from the simulation results that the presence of current leads to a loss of symmetry in flow dynamics for a tension-leg platform (TLP) with symmetric geometry, resulting in the coupling of the heave motion with the surge and pitch motions. Moreover, the presence of current largely affects the wave excitation force and moment as well as the motion of the platform while it has a negligible influence on the added mass and damping coefficients. It is also found that the current effect is strongly correlated with the wavelength but not frequency of the wave field. The global motion of a floating body in the presence of a slow current at relatively small encounter wave frequencies can be satisfactorily approximated by the response of the body in the absence of current at the intrinsic frequency corresponding to the same wavelength as in the presence of current. This finding has a significant implication in the model test of global motions of offshore structures in ocean waves and currents.

Keywords: wave-current-body interaction; platform motions; quadratic boundary element method

1. Introduction

Current generally exists in the ocean environment. For example, post Katrina wave data shows that the current speed can be around 2 m/s in the Gulf of Mexico. Such a current can interact with surface waves and offshore platforms to affect the global motion and safety of the platforms. Therefore, it is of fundamental interest and practical importance to study the hydrodynamic problem of wave-current-body interactions, which is the focus of this paper.

Nakos and Sclavounos (1988) developed a Rankine panel method, based on the unified slender body and slow Froude number theory, to study the three-dimensional steady and unsteady wave-current-body interaction problem in the frequency domain. Kring (1994) extended this work to the time domain. Emmahoff and Sclavounos (1992) analytically studied the current effect for an

*Corresponding author, Senior Research Scientist, E-mail: yuming@mit.edu

^a Email: mshen@mit.edu

infinitely-deep single cylinder and an array of such cylinders based on the assumption of small wave steepness and slow current. The extension of the analytic solution to truncated cylinders or general offshore platforms (such as tension-leg platforms) is not available.

Kim and Kim (1997) applied a high-order boundary element method in the time domain to study the current effect on the motion of a platform. The mathematical formulation was developed based on the assumption of small wave steepness and slow Froude number. The study was focused on the prediction of the mean drift force and wave drift damping of the platform while the current effect on the hydrodynamic coefficients and global motions of the platform was not addressed.

The main objective of this work is to understand the slow current (~ 2 m/s) effect on the global motion of a floating platform in response to the action of surface waves. A time-domain quadratic boundary element method is applied to solve the problem. No approximation with current speed is made in the formulation. The numerical simulation is valid for arbitrary body geometry and finite current speed within the context of potential flow theory. The viscous effects associated with skin friction on body surface at low Reynolds number as well as flow separation at large Keulegan-Carpenter number are not accounted for in this study. The viscous effects might be important in the prediction of hydrodynamic loads and motions of the platforms under realistic ocean environments.

The paper is arranged in the following way. The quadratic boundary element method is introduced in section 2. The numerical results for a truncated circular cylinder including validations by comparisons with the WAMIT prediction (in the absence of current) are shown in section 3. Section 4 presents the detailed simulation results to show the current effects on the added mass, damping, and wave excitation coefficients as well as the free-body motion of a tension-leg platform in waves. The effects of encounter frequency versus intrinsic frequency of the waves on the motion of the TLP are investigated and discussed in section 5. The conclusion is drawn in section 6.

2. Numerical method

The potential flow formulation is employed to describe the interaction problem of a floating body responding to the action of surface waves in the presence of a constant uniform current. The current is assumed to move along the x -direction. The total velocity potential Φ is decomposed as

$$\Phi(\vec{x}, t) = \phi(\vec{x}, t) + Ux$$

where $\vec{x} = (x, y, z)$, ϕ is the disturbance potential and U is the speed of current. Here ϕ represents the effects of blunt-body disturbances from both the steady current and unsteady incident waves. Without loss of generality, we assume that the current moves along the positive x direction. At any time t , the disturbance potential satisfies the Laplace equation in the flow field

$$\nabla^2 \phi = 0, \quad z \leq \eta$$

where $\eta(x, y, t)$ represents the free surface elevation. The linearized free-surface dynamic and kinematic boundary conditions are written as

$$\begin{aligned} \phi_t + U\phi_x + g\eta &= 0, \quad z = 0 \\ \eta_t + U\eta_x - \phi_z &= 0, \quad z = 0 \end{aligned}$$

where g is the gravitational acceleration, and the linearized body boundary condition is

$$\nabla\phi \cdot \vec{n}_0 + U(n_{01} + \xi_5 n_{03} - \xi_6 n_{02}) = \sum_{i=1}^6 \dot{\xi}_i n_{0i}$$

where $\vec{n}_0 = (n_{01}, n_{02}, n_{03})$ and $\vec{x} \times \vec{n}_0 = (n_{04}, n_{05}, n_{06})$ with \vec{n}_0 being the unit normal on the mean body surface pointing into the body (i.e., out of the fluid), $\xi_{1,2,3}$ represents the three translational motion components of the body while $\xi_{4,5,6}$ represent the three rotational motion components, and the symbol ‘ $\dot{\cdot}$ ’ on top of ξ denotes the time derivative. The linearized body boundary condition is applied at the mean position of the body surface. In the far field, a radiation condition that the body disturbance propagates away from the body is imposed. The global motion of the body is governed by Newton’s second law.

A quadratic boundary element method (QBEM) is applied to solve the above stated wave-current-body interaction problem in the time domain (Liu *et al.* 2001, Yan 2010). In this approach, two major steps of computational procedure at each time t are encountered: (I) solve the boundary-value problem for the unknown vertical velocity ϕ_z on the mean free surface and unknown potential ϕ on the body surface for given ϕ on the mean free surface and given body velocity on the mean body surface; and (II) evaluate the total force and moment acting on the body and integrate the equation of motion for the body forward with time to obtain the velocity and position of the body at new time $t + \Delta t$, and integrate the evolution equations (i.e. the dynamic and kinematic free-surface boundary conditions) forward in time to update the free-surface position $\eta(t + \Delta t)$ and the velocity potential $\phi(t + \Delta t)$. The time simulation of the wave-current-body interaction problem up to any specified time is achieved by repeating these two steps of computational processes starting from the appropriate initial conditions.

In solving the boundary-value problem in step (I), the solution of ϕ to the boundary-value problem is obtained from the use of Green’s identity

$$\alpha\phi(\vec{x}) = - \iint_{\partial B + \partial F} [\phi(\vec{x}')G_n(\vec{x}; \vec{x}') - \phi_n(\vec{x}')G(\vec{x}; \vec{x}')] ds(\vec{x}')$$

where α is the solid angle, G is the Rankine source Green function, \vec{n} is the surface normal pointing out of the fluid, and ∂B represent the mean body surface while ∂F represents the mean free surface. When the field point is fixed on the mean free surface and body surface, the boundary integral equation for unknown ϕ_z on ∂F and unknown ϕ on ∂B is resulted. QBEM is employed to solve this boundary integral equation.

The pressure is obtained through Bernoulli equation

$$p(\vec{x}, t) = -\rho(\phi_t + U\phi_x + gz)$$

where ρ is the fluid density. The force \vec{F} and moment \vec{M} on the body are obtained by

$$\vec{F} = \iint_{\partial B} p\vec{n} ds \quad \text{and} \quad \vec{M} = \iint_{\partial B} p(\vec{r} \times \vec{n}) ds$$

where \vec{r} represents the arm of the moment with respect to the center of rotation. The forth-order Rounge-kutta integration scheme is used to integrate the equation of motion for body and the free-surface evolution equations forward with time. The upwind finite-difference scheme is used in

the evaluation of the horizontal velocity ϕ_x on the mean free surface. This ensures the instability in time integration in the presence of current.

A sponge layer in a narrow strip of the free surface is added in the far field of the computational domain to absorb the outgoing waves (Yan 2010). The free surface boundary conditions in the sponge layer take the form

$$\begin{aligned}\phi_t &= -U\phi_x - g\eta - \frac{\nu}{k}\phi_z, \quad z = 0 \\ \eta_t &= -U\eta_x - \phi_z - \nu\eta, \quad z = 0\end{aligned}$$

where $\nu(x, y)$ is the artificial damping coefficient which is generally a function of space.

3. Results of a truncated vertical circular cylinder

A truncated vertical circular cylinder is first considered. The draft of the cylinder $H=27.4$ m and the radius $R=10.8$ m. Deep water is assumed. A schematic sketch of the problem is shown in Fig. 1. A circular computational domain is chosen with a radius of 30 cylinder radius. Axial symmetric grids are used. On the free surface, 25 uniform grids in the polar direction and 71 uniform grids in the radial direction are used. In the sponge layer, $\nu(x, y)$ linearly increased from zero to $\nu_{\max} = \omega$ in the radial direction of the computational domain, where ω is the incident wave frequency.

3.1 Diffraction problem

For the diffraction problem, the total disturbance velocity potential is decomposed into the incident potential ϕ_I and diffraction potential ϕ_D . The diffraction potential ϕ_D is unknown while the incident potential ϕ_I is specified. For the diffraction problem, the body is fixed. The boundary condition for ϕ_D on the body surface becomes

$$\nabla\phi_D \cdot \vec{n}_0 + Un_{01} = -\nabla\phi_I \cdot \vec{n}_0$$

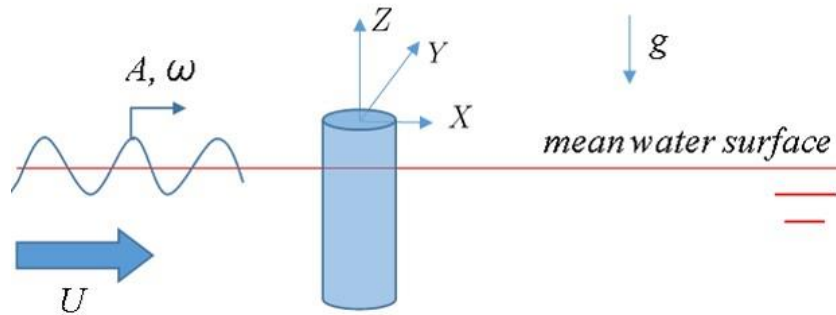


Fig. 1 Schematic sketch of the wave-current-body interaction problem

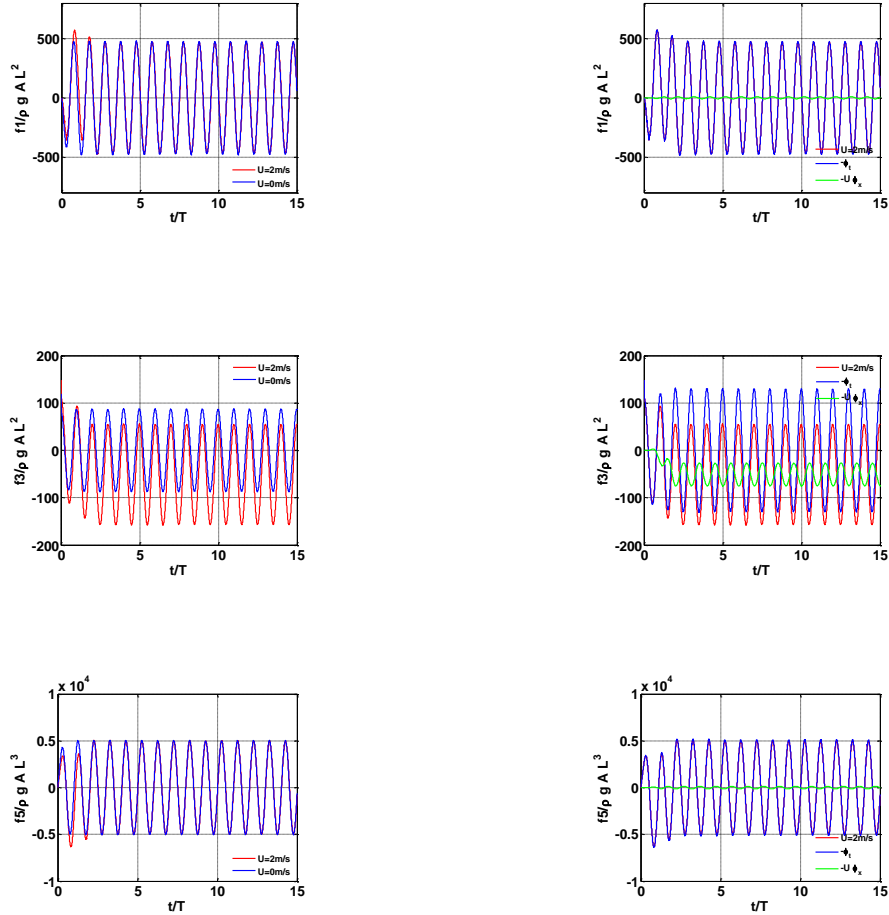


Fig. 2 Left panels: time histories of the surge ($f1$) and heave ($f3$) forces and pitch ($f5$) moment on a stationary vertical circular cylinder in a regular wave with and without the presence of current $U=2$ m/s. Right panels: time histories of the surge and heave forces and pitch moment on the cylinder due to different pressure components in the case of $U=2$ m/s. (The length scale $L=1$ m)

Consider a regular incident wave with a wave period of $T=10$ s. To see the current effect, we compare the results obtained with $U=0$ and $U=2$ m/s. In the case of non-zero U , the encounter wave period is used. Fig. 2 shows the time histories of the surge and heave forces as well as pitch moment on the cylinder. The results with $U=0$ and $U=2$ m/s are compared. It is seen that the presence of current slightly increases the amplitude of the first-harmonic heave force ($f3$) despite the fact that the contribution to $f3$ from the pressure component $U\phi_x$ is out of the phase with that from ϕ_t . (One notes that the contribution to $f3$ from ϕ_t in the case of $U=2$ m/s is significantly larger than that in the case of $U=0$). In addition, a negative mean force of $f3$ is resulted from the action of U , which is as expected in the steady flow problem (i.e. without the presence of unsteady waves).

On the other hand, the presence of current does not have an apparent effect on the surge force (f_1) and pitch moment (f_5) since the contributions from the pressure component $U\phi_x$ to f_1 and f_5 are negligibly small.

The steady-state amplitude and phase of the surge and heave forces and pitch moment for a range of wave periods [7s-18s] are shown in Fig. 3. Over this range of wave periods, the presence of current exhibits the same qualitative effect on f_1 , f_3 and f_5 as described in the above (for $T=10$ s). In the case of $U=0$, the present results match well with those by the commercial tool WAMIT, validating the present computations.

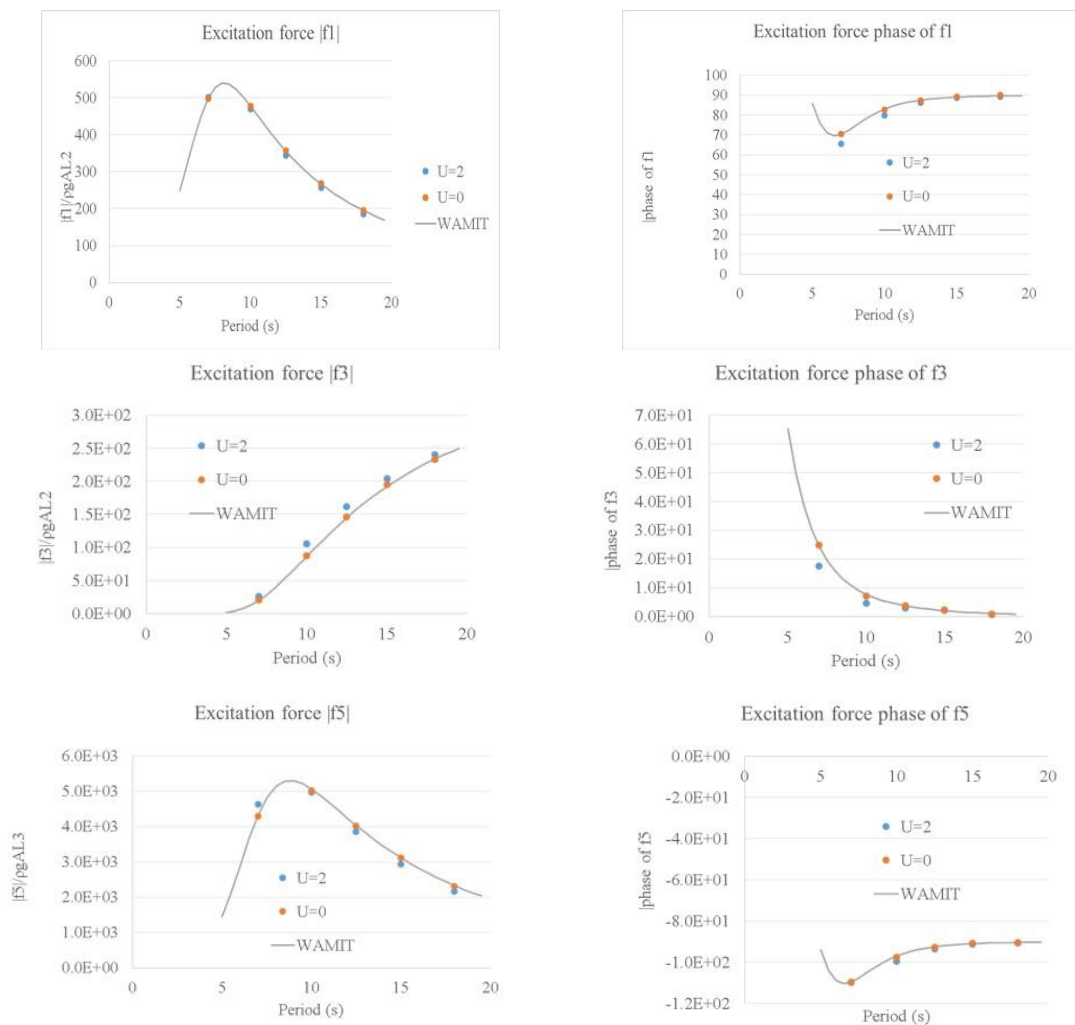


Fig. 3 The amplitude (left panel) and phase (right panel) of the surge (f_1) and heave (f_3) forces and pitch moment (f_5) on a stationary truncated vertical circular cylinder in waves with and without current ($U=2$ m/s). The result from the commercial tool WAMIT in the case of no current is shown for comparison. (The length scale $L=1$ m)

3.2 Radiation problem

In the radiation problem, the cylinder is forced to undergo a specified time-periodic oscillation in the absence of ambient waves. The purpose is to investigate the current effect on the added mass and wave damping coefficients. The body boundary condition for the radiation potentials ϕ_{Rj} , $j = 1,3,5$, is given by

$$\nabla \phi_{Rj} \cdot \vec{n}_0 + U(n_{01} + \delta_{5,j} \xi_5 n_{03}) = \dot{\xi}_j n_{0j}$$

where ξ_j , $j = 1,3,5$, is the specified surge, heave and pitch motions of the cylinder, and $\delta_{i,j}$ is the Kronecker delta function. The added mass and damping coefficients can be obtained from the resulting hydrodynamic force and moment on the body.

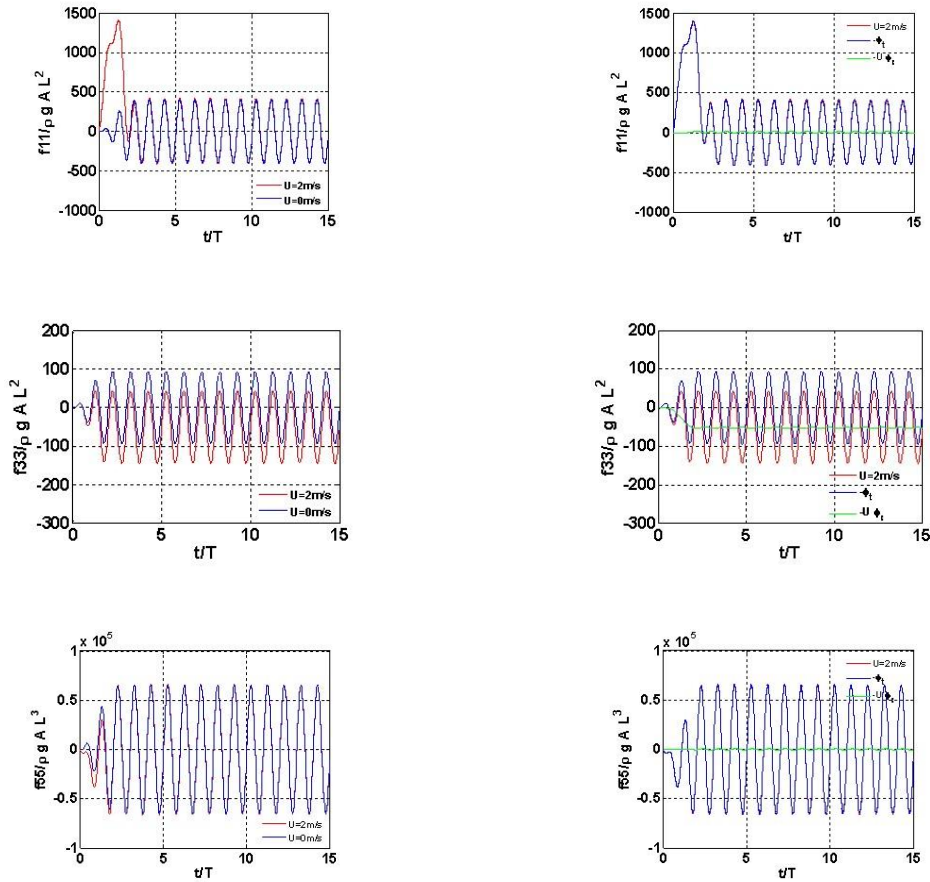


Fig. 4 Left panels: time histories of the radiation surge and heave forces, f_{11} and f_{33} , and pitch moment, f_{55} , of a truncated vertical circular cylinder at forced motion period $T=10\text{s}$ with and without the presence of current ($U=2\text{ m/s}$). Right panels: time histories of f_{11} , f_{33} and f_{55} due to different pressure components in the presence of current. (The characteristic length scale $L=1\text{ m}$)

Fig. 4 shows the time history of the radiation forces (f_{11} and f_{33}) and moment (f_{55}) with the forced motion period $T=10$ s. The current effect on the harmonic components of these forces and moment, which are associated with the diagonal elements of the added mass and damping matrices, is negligibly small since the contributions to these forces and moment from the pressure component $U\phi_x$ is near zero, as shown in Fig. 4. The diagonal components of the added mass and damping matrices (A11, B11, A33, B33, A55, B55) with and without the presence of current for a wide range of periods are shown in Fig. 5. Similarly to the result at $T=10$ s, the current effect on these components is negligible.

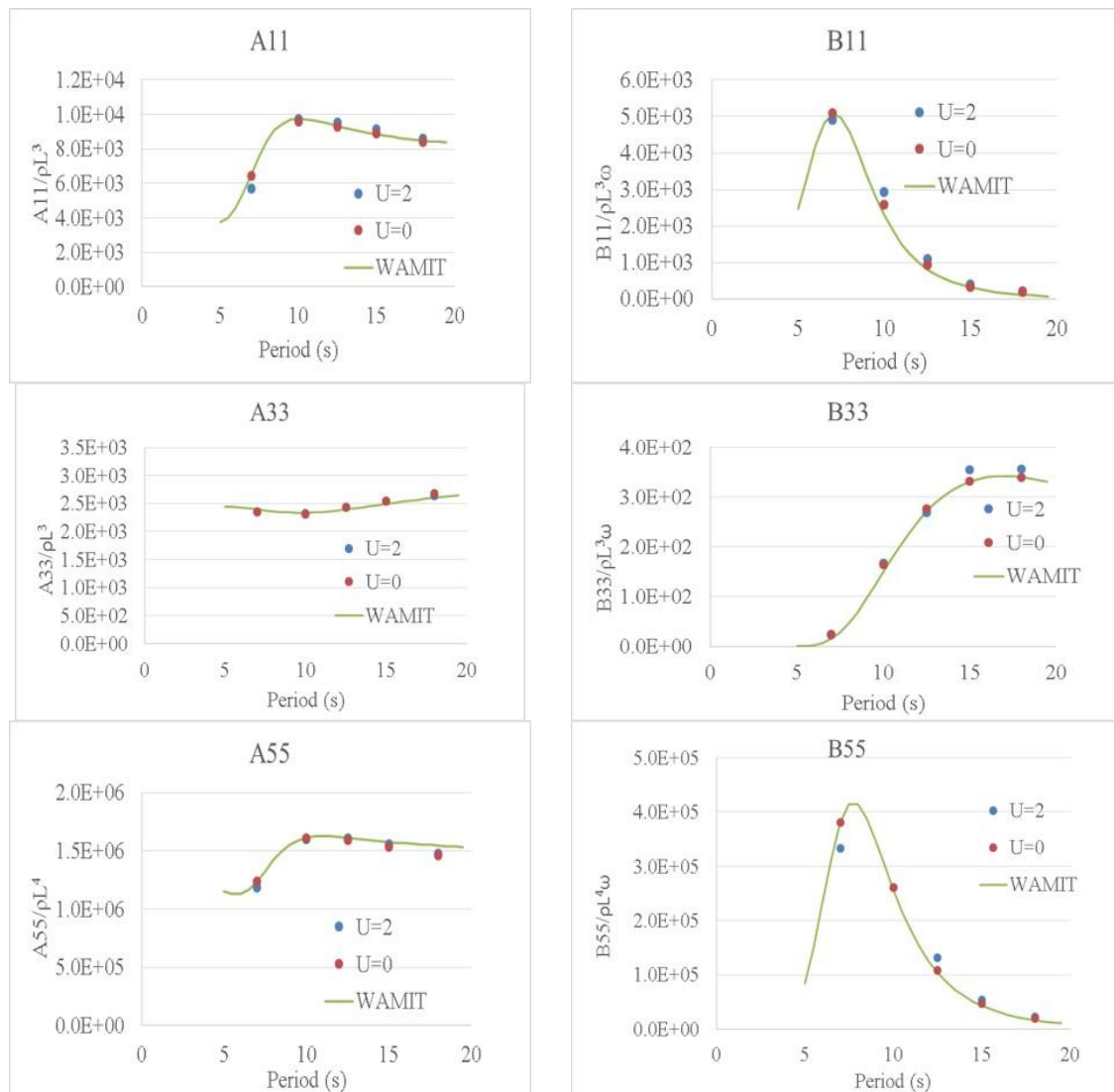


Fig. 5 Comparisons of the diagonal elements of the added mass and damping coefficient matrices of a truncated vertical circular cylinder with and without the presence of current ($U=2$ m/s). The prediction by the commercial tool WAMIT in the case of no current is shown for validation. (The length scale $L=1$ m)

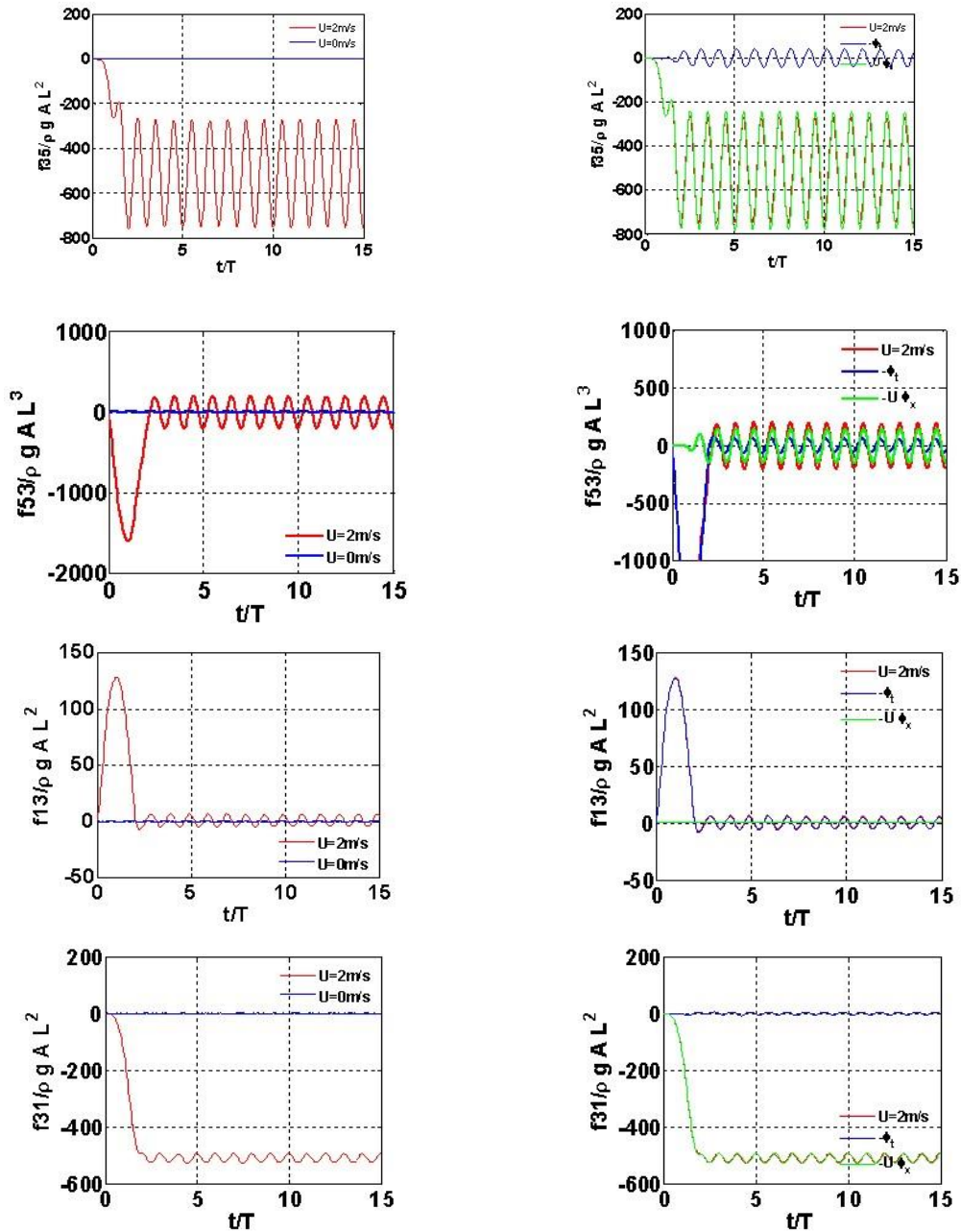


Fig. 6 Left panels: time histories of the radiation forces and moments, f_{35} , f_{53} , f_{13} , and f_{31} , of a truncated vertical circular cylinder at forced motion period $T=10\text{s}$ with and without the presence of current ($U=2\text{ m/s}$). Right panels: time histories of these forces and moments due to different pressure components in the presence of current. (The characteristic length scale $L=1\text{ m}$)

In the presence of current, the force and moment (f_{13} , f_{31} , f_{35} , and f_{53}) associated with off-diagonal elements of the added mass and damping matrices become non-zero, as shown in Fig. 6. These force and moment are zero in the absence of current since the heave motion is uncoupled with the surge and pitch motions due to symmetry of body geometry. The non-zero contributions are mainly from the pressure component $U\phi_x$ from the current effect. In the presence of current, f_{13} is not equal to f_{31} , and f_{35} is not equal to f_{53} , as Fig. 6 shows. The current effect on the forces f_{15} and f_{51} is negligible. The analysis of our numerical simulation results (with $T=10$ s and $U=\pm 2$ m/s) also indicates that the cross coupling added mass and damping coefficients in the presence of small U satisfy the Timman-Newman relation (such as $A_{13}(U)=-A_{13}(-U)$, $B_{13}(U)=-B_{13}(-U)$). (The differences between the corresponding terms are all less than 10%).

3.3 Free response

In the free response problem with and without the presence of current, the cylinder freely oscillates in response to the action of incident waves. The weight of the truncated vertical circular cylinder is assumed to be equal to the buoyance. The center of gravity is assumed to be at the center of the cross section of the body on the mean free surface $(0, 0, 0)$. The natural periods of heave and pitch motions are made to be 2.85 s and 3.10 s, respectively. The natural period of surge is set to be 130 s by adding an artificial spring.

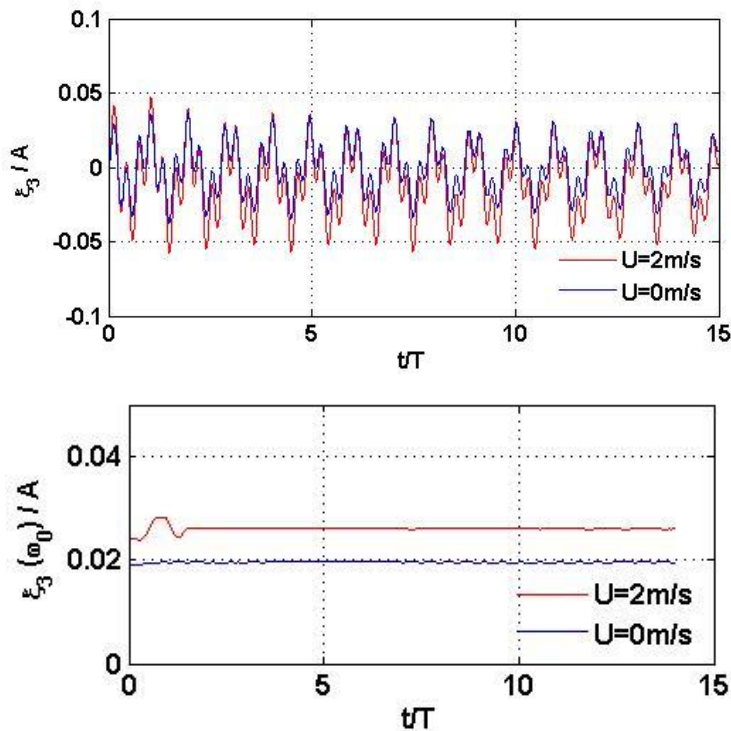


Fig. 7 Time histories of the heave motion (top) and corresponding heave motion amplitude (bottom) (at the wave frequency) of the truncated vertical circular cylinder in regular waves with period $T=10$ s with and without the presence of current $U=2$ m/s

The free-body heave response of the truncated cylinder at the incident wave period $T=10$ s is shown in Fig. 7. Due to slow decay of natural-mode motion (associated with the initial transient effects, the time records of the body motion show clear modulation behavior as a result of the sum of the natural frequency and wave frequency body motions. By using the Fourier decomposition with a moving time window, the amplitudes of the wave frequency motion and natural-frequency motion can be separated. In Fig. 7, the time history of the amplitude of the wave-frequency heave motion (normalized by the incident wave amplitude A) is also displayed. It is seen that the presence of current ($U=2$ m/s) increases the heave motion by about 30% compared to the case without current. The current effect on the surge and pitch motions is found to be negligible. (We note that the predicted body motions with $T=10$ s in the absence of current match the WAMIT results very well).

4. Results of a Tension-Leg Platform (TLP)

The TLP has four columns and four pontoons. The dimensions of the TLP are shown in Table 1. Since the ratio of draft and radius is not large, the pontoon effect cannot be ignored in the wave period range [3-20s]. Fig. 8 shows the sample discretization of the underwater TLP surface and the free surface for QBEM computations. For the results presented below, the heading of the incident wave and current is along the side direction of the TLP. Due to the symmetry of body geometry with respect to the wave/current direction, the TLP undergoes non-zero surge, heave and pitch motions only. The center of the gravity of the TLP is at 16.2 m above the mean water surface. The pitch motion presented below is obtained with respect to the center of gravity of the TLP. The TLP's mass and mooring properties are chosen such that the natural periods of the surge, heave and pitch motions are 128s, 3.55s and 3.60s, respectively, which are similar to the values of realistic TLPs.

For the diffraction problem, Fig. 9 compares the diffraction force and moment on the TLP at an incident wave period of $T=10$ s with and without the presence of current ($U=2$ m/s). Unlike for the truncated circular cylinder, the presence of current significantly affects the diffraction force and moment on the TLP. Specifically, for the surge force and pitch moment, both the first-harmonic and mean components are significantly increased due to the current effect. For the heave force, a negative mean force is produced by the current effect while the first-harmonic component remains nearly unchanged. The effect on the mean (or first-harmonic) components is due to contributions from the pressure component $U\phi_x$ (or ϕ_t).

Table 1 Dimensions of the TLP

Column	(m)
Radius (R)	10.8
Draft	27.4
Pontoon	
Width	10.4
Height	10.4
Length (Lcc)	62.2

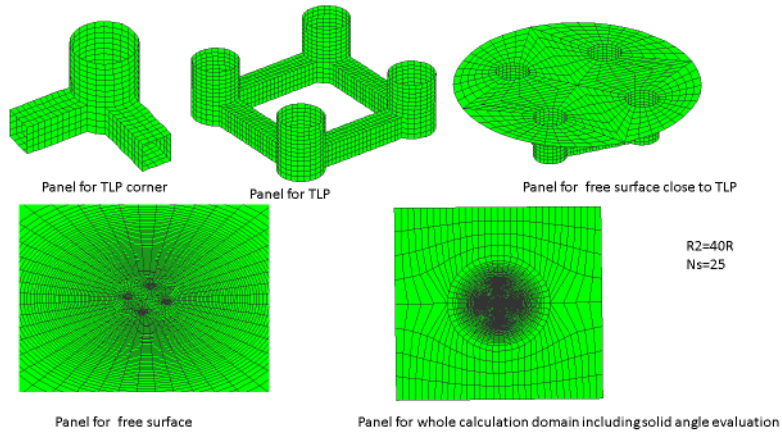


Fig. 8 Sample discretization of the TLP-body surface and free surface for QBEM computations

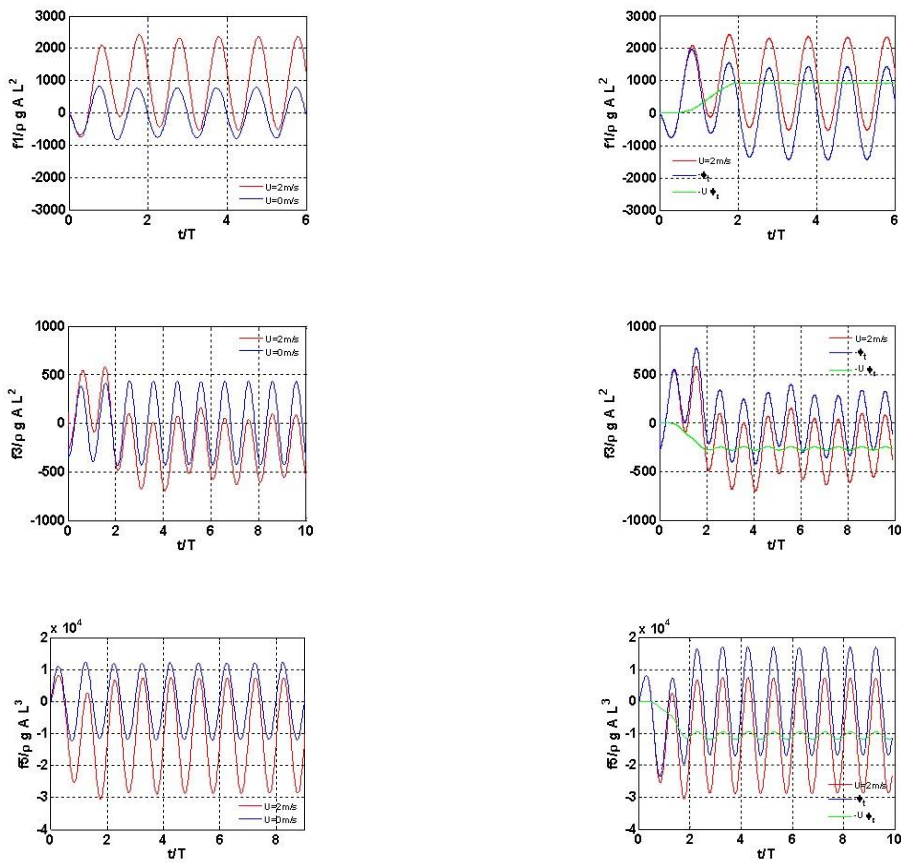


Fig. 9 The current effect on the diffraction forces and moment of the TLP with incident wave period $T=10s$. (The length scale $L=1m$)

For the radiation problem, figure 10 displays the time histories of the diagonal radiation forces (f_{11} , f_{33} , f_{55}) and the contributions to these forces from each pressure component. For the forced motion period $T=10$ s, the presence of current does not have a meaningful effect on the harmonic radiation forces. The off-diagonal radiation forces (f_{13} , f_{31} , f_{35} , f_{53}) are shown in Fig. 11. As in the case of a truncated vertical circular cylinder, the presence of current causes the coupling of heave mode with surge and pitch modes, leading to significant non-zero values of f_{13} , f_{31} , f_{35} and f_{53} . They are uncoupled in the absence of current due to symmetry of body geometry. As in the case of a vertical truncated circular cylinder case, the current effect on f_{15} and f_{51} is negligible.

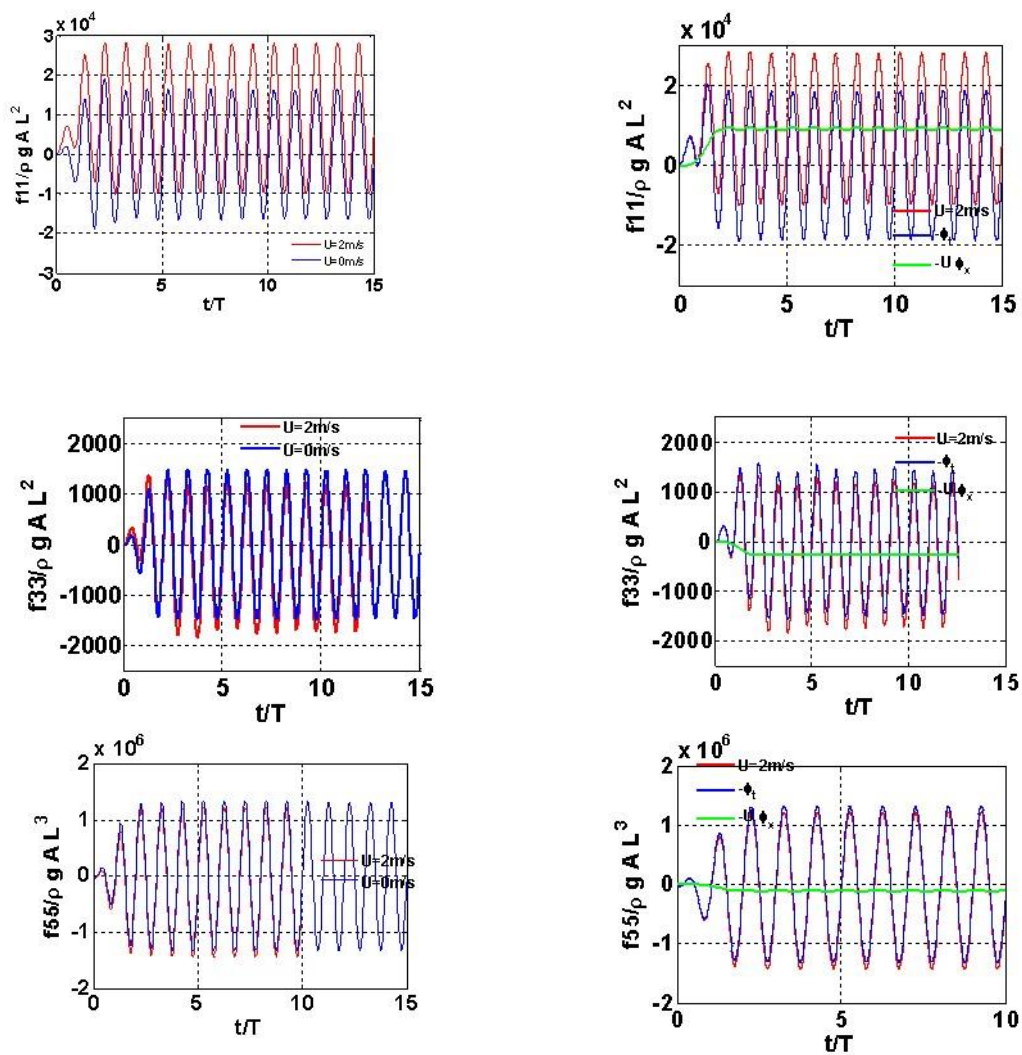


Fig. 10 Time histories of the diagonal radiation forces of the TLP at period $T=10$ s. (The characteristic length scale $L=1$ m)

The amplitudes of the free-body motions of the TLP in the incident wave period range of [7s-18s] is presented in Fig. 12, where the results with $U=2$ m/s, 0, and -2 m/s are compared. For the surge and pitch responses, current has apparent effects for encounter wave period $T_e=[7s-13s]$. The current effect is negligible for encounter wave period greater than 14s. For the heave motion, current can have significant effects in the whole range of $T_e=[7s-18s]$. The cancellation concave shifts with the current.

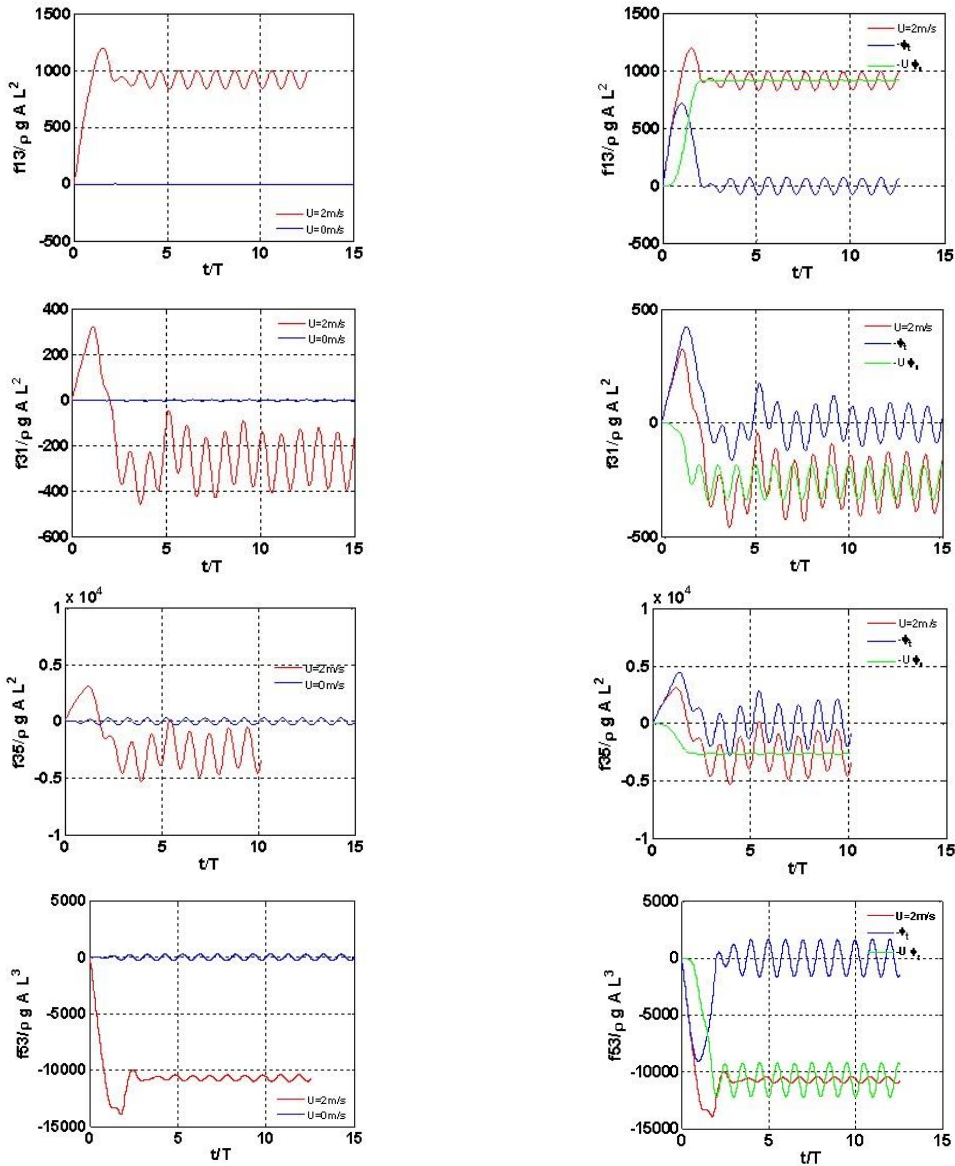


Fig. 11 Time histories of the off-diagonal radiation forces of the TLP at period $T=10$ s. (The characteristic length scale $L=1$ m)

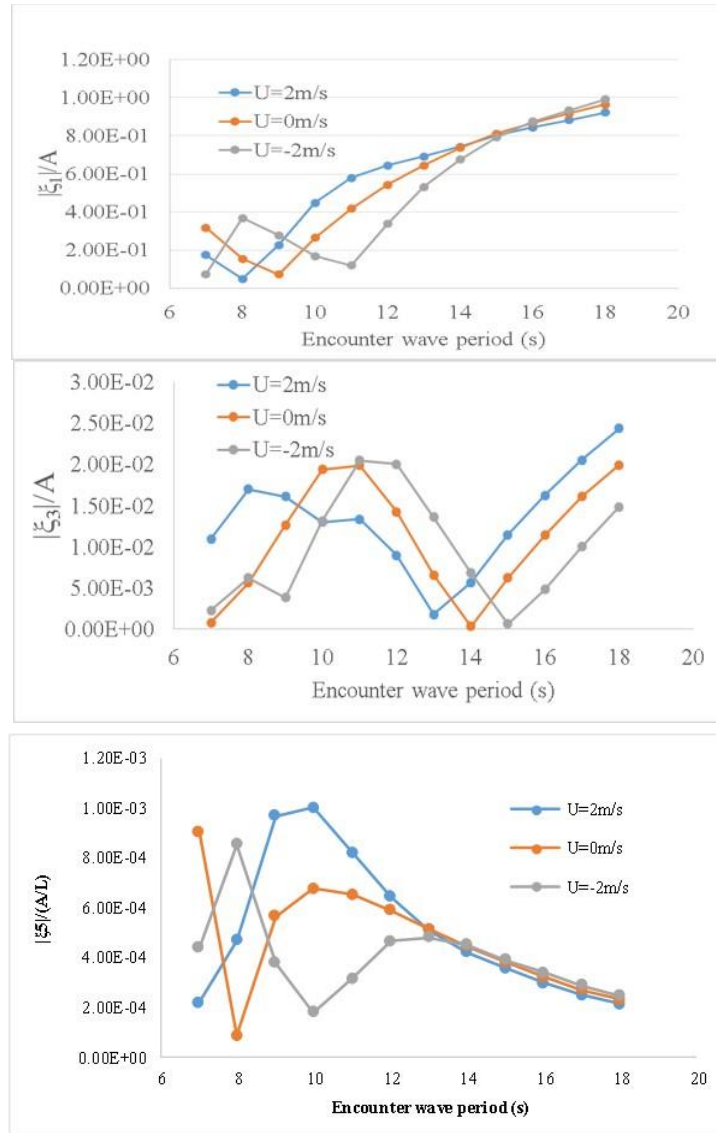


Fig. 12 Comparisons of the free body response of the TLP as a function of encounter incident wave period in the presence of current with $U=2$ m/s, 0, and -2 m/s. (The length scale $L=1$ m)

5. Intrinsic versus apparent free-body response

The global motion of a floating body in waves can be significantly influenced by current. Especially for large encounter periods, the presence of current (with positive speed) shifts the response curve to the higher periods. In order to better understand the current effect on the body motion, we compare the results based on the encountered period (also called apparent period) with those obtained based on the so-called intrinsic wave period (or wavelength). Using the result from

the intrinsic wave period to account for the current effect is often employed in experiments. It is of importance to assess the accuracy and validity of this ad-hoc approach.

The encounter frequency ω_e of a wave with wavenumber k in the presence of current is given by the dispersion relation (in deep water)

$$\omega_e = Uk + \sqrt{gk}$$

The intrinsic frequency ω_i of a wave with the same wavenumber k in the absence of current is

$$\omega_i = \sqrt{gk}$$

The encounter frequency is related to the intrinsic period by the relation

$$\omega_e = \frac{U\omega_i^2}{g} + \omega_i$$

Tables 2 lists sample intrinsic wave periods at current speed $U=2$ m/s and -2 m/s corresponding to the given encounter periods. For given encounter wave periods, the wavelengths at different current speed are given in Table 3.

The intrinsic wave period with positive current (i.e., current and wave are in the same direction) is larger than the encounter period and vice versa. At the same encounter frequency, the wavelength becomes larger (smaller) with the presence of positive (negative) current.

In order to see the difference between the intrinsic-frequency response and the apparent-frequency (i.e., encounter-frequency) response, we perform two types of computations. In the first case, for given current speed and encounter wave frequency, we calculate the encounter-frequency response of the body, which is labeled as ‘apparent’ result. In the second case, we calculate the response of the body at the corresponding intrinsic frequency but in the absence of current, which is labeled as ‘intrinsic’ result.

Table 2 The intrinsic vs. encounter wave periods at different current speeds

Encounter period (s)	Intrinsic period (s)	
	U=2 m/s	U=-2 m/s
7.5	8.6	5.9
10	11.1	8.5
12.5	13.7	11.1
15	16.2	13.6
17.5	18.7	16.1

Table 3 Intrinsic wavelength (λ) at different current speeds for given encounter wave period. (Lcc=62.2 m)

Encounter period (s)	λ/L_{cc}		
	(U=0)	(U=2 m/s)	(U=-2 m/s)
7.5	1.4	1.9	0.9
10	2.5	3.1	1.8
12.5	3.9	4.7	3.1
15	5.6	6.6	4.6
17.5	7.7	8.8	6.5

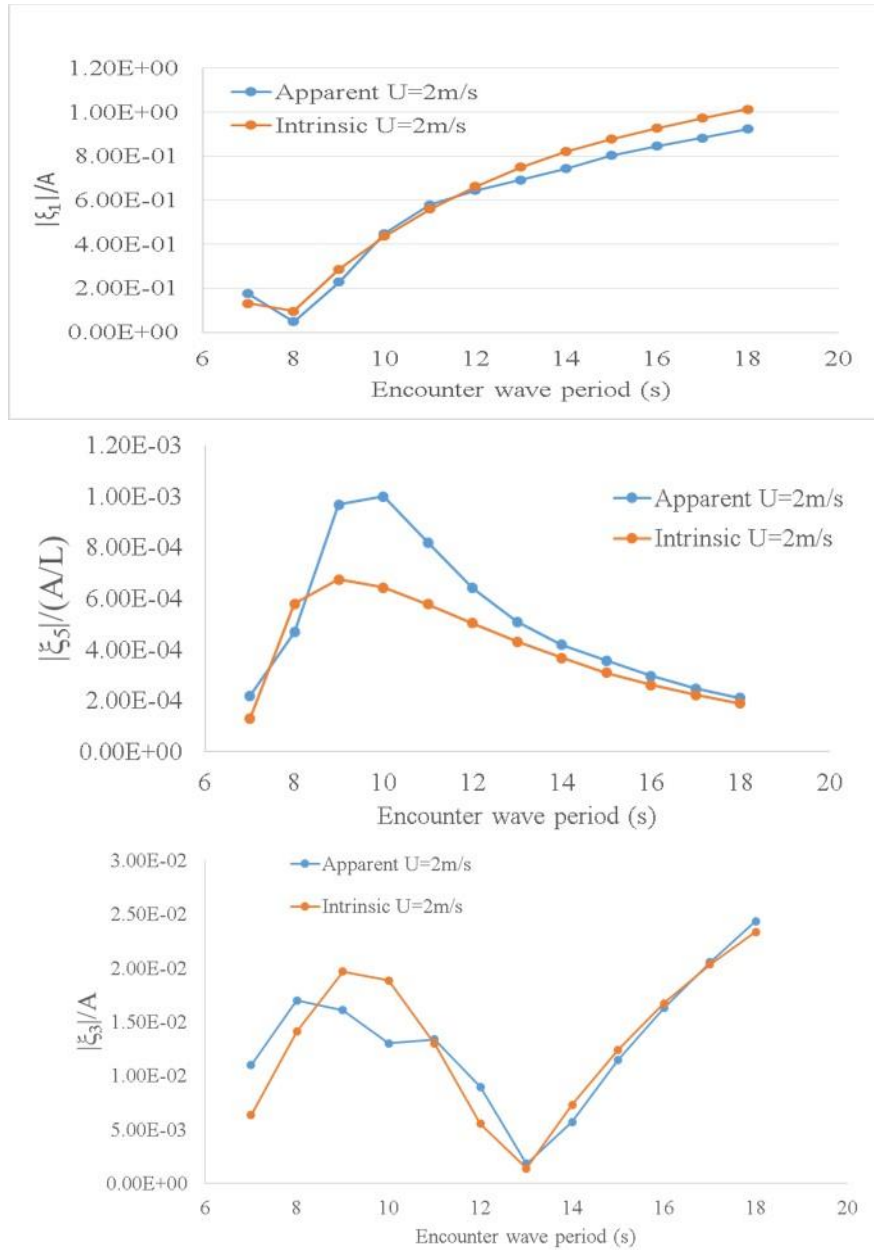


Fig. 13 Comparison of ‘intrinsic’ and ‘apparent’ results of the TLP motion for current speed $U=2\text{m/s}$. (The length scale $L=1\text{ m}$)

Fig. 13 compares the ‘apparent’ and ‘intrinsic’ results of the TLP motion for an encounter period range [7-18s] with current speed $U=2\text{ m/s}$. The similar results for the case of $U=-2\text{ m/s}$ are

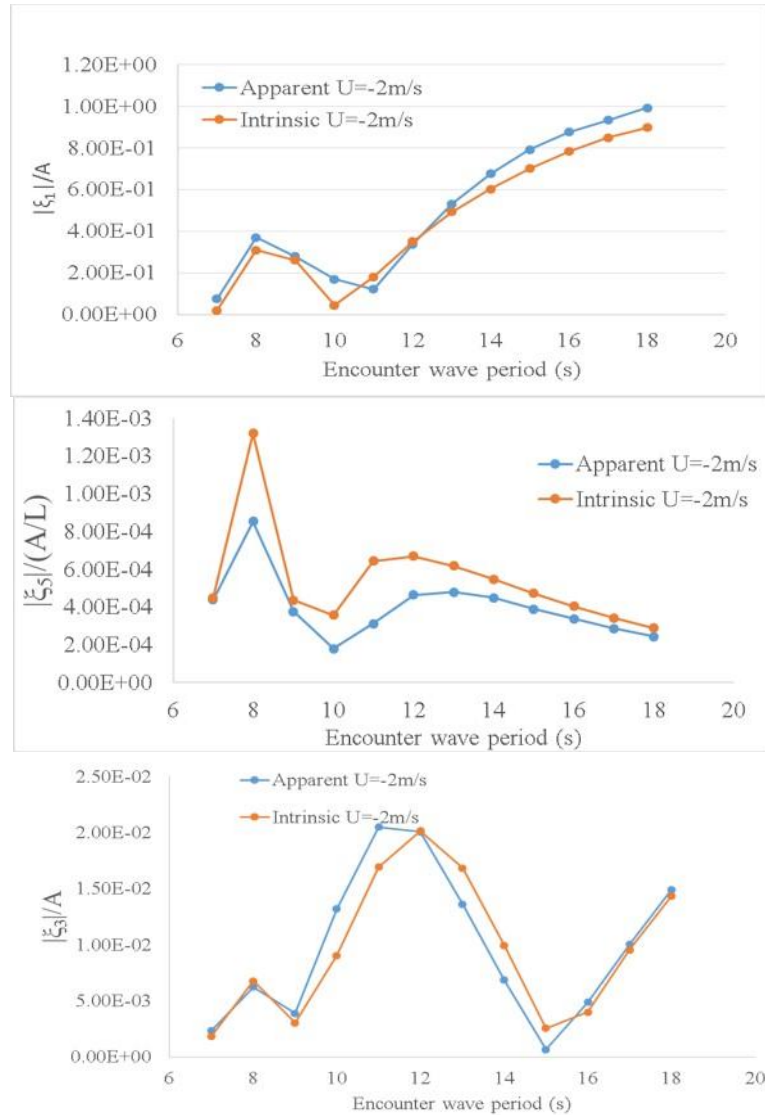


Fig. 14 Comparison of 'intrinsic' and 'apparent' results of the TLP motion for current speed $U=-2$ m/s. (The length scale $L=1$ m)

shown in Fig. 14. In both cases, at large encounter periods ($T_e > \sim 12$ s), the 'intrinsic' result matches the 'apparent' result well for all three modes of TLP motions. At relatively smaller encounter periods ($T_e < \sim 12$ s), distinctive differences between 'intrinsic' and 'apparent' results of the heave and pitch motions are seen while they still match well for the surge motion. In this range of small encounter periods, the wavelength is comparable to the characteristic length L_{cc} of the TLP. Strong wave diffraction effects make it invalid to use the 'intrinsic' result to represent the 'apparent' result.

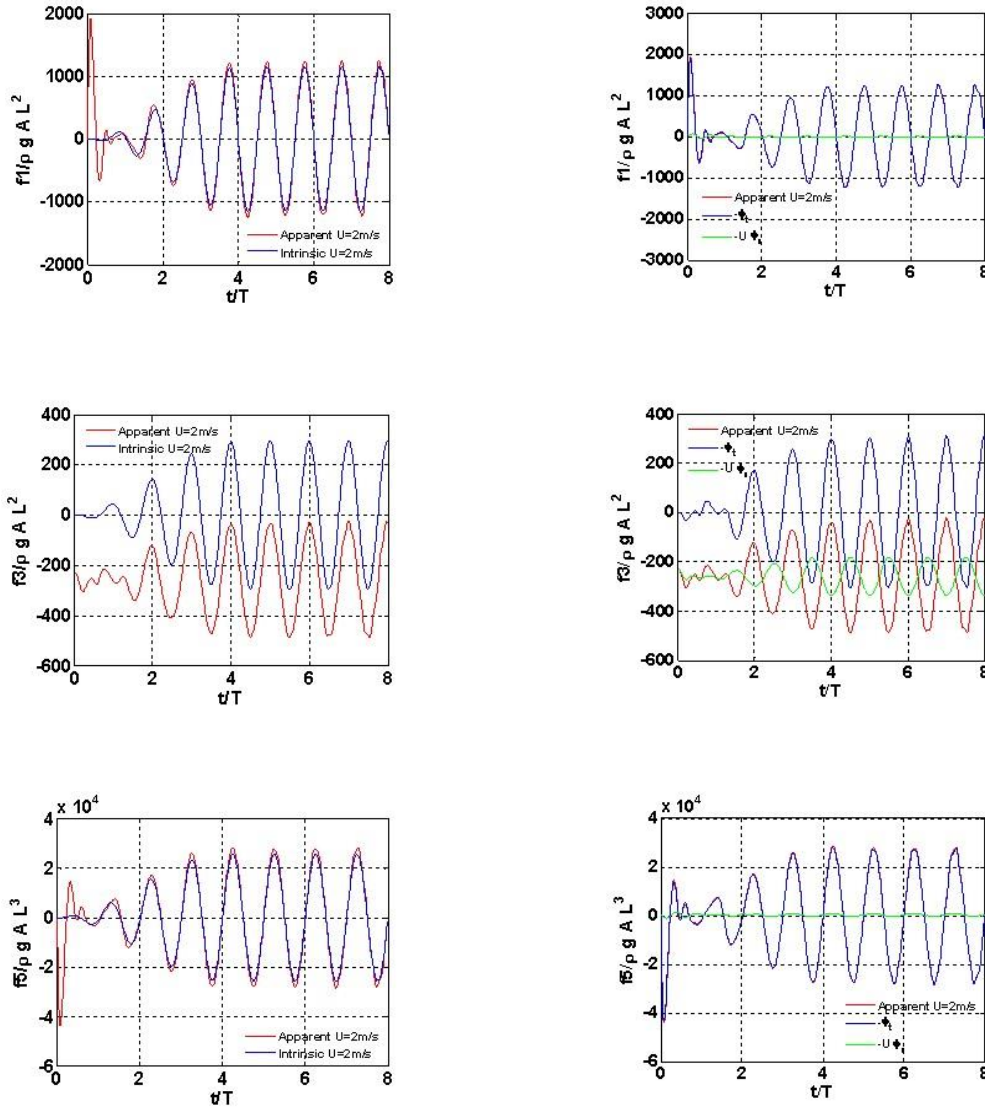


Fig. 15 Comparisons of the diffraction force/moment on the TLP obtained using the intrinsic incident wave and apparent incident wave. The time is normalized by the corresponding intrinsic or apparent wave periods. (Current speed $U=2$ m/s, apparent period $T_e = 15$ s, and length scale $L=1$ m)

A simple mathematic model is used to explain the phenomenon. Consider the dynamic pressure on the body

$$p_d = -\phi_t - U\phi_x$$

$$\phi = \phi_I + \phi_D$$

where ϕ_I is the incident wave potential and ϕ_D is the disturbance wave potential due to the wave diffraction and radiation by the TLP. At large encounter periods, the wavelength is much larger than L_{cc} so that $\phi_I \gg \phi_D$. By neglecting ϕ_D effect, the pressure becomes

$$p_d \approx -\phi_{Iz} - U\phi_{Ix}$$

For a plane incident wave in deep water

$$\phi_I = \frac{-igA}{\omega_0} e^{ikx - i\omega t} e^{kz}$$

which gives the amplitude of the pressure

$$p_d = gA e^{ikx} e^{kz}$$

where A is the incident wave amplitude. Since p_d is a function of wavenumber but not frequency, the resulting exciting force/moment on the body is dominated by the wavenumber effect. Since the intrinsic wave has the same wavenumber as the wave in the presence of current, the ‘intrinsic’ result of the body response compares well with the ‘apparent’ result.

As a verification of the above simple mathematical argument, Fig. 15 compares the diffraction forces on the TLP obtained at the intrinsic and encounter periods. The surge force f_1 and pitch moment f_5 obtained with the intrinsic incident wave (without current) compares well with those obtained with the apparent incident wave (in the presence of current). For the heave force f_3 , the amplitudes of the first-harmonic component by the two approaches are comparable. These results are consistent with the simple mathematical argument.

6. Conclusions

A time-domain numerical simulation based on a quadratic boundary element method is applied to investigate the slow current effects on the global response of floating offshore platforms in waves. The problem is addressed in the context of linearized potential-flow wave theory. The full wave-current-body interactions are considered. The wave excitations, added mass and damping coefficients, and free responses of the body with and without the presence of current are computed and compared. It is found that the presence of current can significantly affect the wave excitations on the body causing distinctive differences in the prediction of the global response of the body. In addition, the presence of current causes the loss of flow symmetry leading to additional coupling of body motion modes. For example, the uncoupled heave mode with surge and pitch modes of a TLP in the absence of current will become fully coupled in the presence of current. It is found that it is the wavelength (or wavenumber) rather than the wave frequency that controls the current effect on the excitations and responses of the TLP since the spatial variation of the flow dominates the dynamic pressure field. The motion of a floating platform in the presence of current can be reasonably approximated by the prediction in the absence of current with the use of intrinsic frequency that corresponds to the same wavelength as in the presence of current. This

approximation is shown to be reasonably accurate at relatively low wave frequencies (or long wavelengths).

References

- Emmerhoff, O.J. and Slavounos, P.D. (1992), "The slow-drift motion of arrays of vertical cylinders", *J. Fluid Mech.*, **242**, 31-50.
- Kim, D.J. and Kim, M.H. (1997), "Wave-current interaction with a large three-dimensional body by THOBEM", *J. Ship Res.*, **41**(4), 273-285.
- Kring, D.C. (1994), "Time domain ship motions by a three-dimensional Rankine panel method", Ph.D. Dissertation, Massachusetts Institute of Technology, Massachusetts.
- Liu, Y., Xue, M. and Yue, D.K.P. (2001), "Computations of fully nonlinear three-dimensional wave-wave and wave-body interactions. Part 2. Nonlinear waves and forces on a body", *J. Fluid Mech.*, **438**, 41-66.
- Nakos, D.E. and Slavounos, P.D. (1989), "On steady and unsteady ship wave patterns", *Fluid Mech.*, **215**, 263-288.
- Yan, H. (2010), "Computations of Fully Nonlinear Three-dimensional Wave-Body Interactions", Ph.D. Dissertation, Massachusetts Institute of Technology, Massachusetts.
- Yan, H. and Liu, Y. (2011), "An efficient high-order boundary element method for nonlinear wave-wave and wave-body interactions", *J. Comput. Phys.*, **230**(2), 402-424.

MK